AIP Advances

Control of metal-insulator transition temperature in VO_2 thin films grown on RuO_2/TiO_2 templates by strain modification

Cite as: AIP Advances **9**, 015302 (2019); https://doi.org/10.1063/1.5083848
Submitted: 30 November 2018 . Accepted: 30 December 2018 . Published Online: 09 January 2019

H. Kim, N. A. Charipar, J. Figueroa, N. S. Bingham, and A. Piqué

Control of metal-insulator transition temperature in VO_2 thin films grown on RuO_2/TiO_2 templates by strain modification

Cite as: AIP Advances 9, 015302 (2019); doi: 10.1063/1.5083848
Submitted: 30 November 2018 • Accepted: 30 December 2018 •
Published Online: 9 January 2019

H. Kim,[1,a)] N. A. Charipar,[1] J. Figueroa,[1] N. S. Bingham,[2] and A. Piqué[1]

AFFILIATIONS

[1] Naval Research Laboratory, Washington, District of Columbia 20375, USA
[2] National Research Council Fellow at the Naval Research Laboratory, Washington, District of Columbia 20375, USA

[a)] Author to whom correspondence should be addressed: heungsoo.kim@nrl.navy.mil

ABSTRACT

Ruthenium dioxide (RuO_2) is an ideal buffer layer for vanadium dioxide (VO_2) heterostructures due to its high electrical conductivity and matching crystal structure with metallic VO_2. VO_2 thin films were deposited on single crystal TiO_2 (001) substrates with RuO_2 buffer layers via pulsed laser deposition. The metal-insulator transition temperature (T_{MIT}) in VO_2 films can be controlled by the epitaxial strain between the VO_2 film and RuO_2 buffer layer by adjusting the buffer layer thickness (10 - 50 nm). We observed a decrease in the T_{MIT} of VO_2 films from 59 °C to 24 °C as the RuO_2 thickness decreased from 50 nm to 10 nm. Additionally, we show that the RuO_2 buffer layer can sustain an intermediate strain state in VO_2 films up to 100 nm in thickness with a subsequently lower T_{MIT} (30 °C). The 10 nm thick RuO_2 buffer layer can reduce the T_{MIT} in VO_2 films by providing a pathway to relieve the strain through grain boundaries.

I. INTRODUCTION

Vanadium dioxide (VO_2) undergoes a sharp metal-insulator transition (MIT) above room temperature at ~67 °C, which is associated with a structural phase transformation (SPT) between a low-temperature insulating monoclinic phase and a high-temperature metallic tetragonal phase.[1] The MIT and SPT can be controlled by external parameters such as temperature,[2] electric field,[3] or photo-excitation,[4] and the switching time of the transition can be on ultrafast timescales (~100 fs) when the transition is induced optically.[5,6] As the temperature of the VO_2 increases above 67 °C, the electrical resistivity decreases by several orders of magnitude and the infrared transmittance decreases by ~60 %.[7] These unique properties have made VO_2 an attractive candidate in many promising applications such as ultrafast switches,[8,9] thermo-optical modulators,[10] field effect transistors,[11,12] bolometric photodetection,[13] plasmonic metamaterials,[14] thermal actuators,[15] and smart radiators for spacecraft.[16]

The nature of the MIT and SPT in VO_2 has been a long-standing debate. It is generally acknowledged that the mechanism of the MIT in bulk VO_2 is considered to be a collaborative Mott-Peierls transition. The SPT from monoclinic (M1) phase to tetragonal rutile (R) phase is most commonly reported; however, some intermediate phases, such as M2-phase,[17,18] B-phase,[19] A-phase,[19] have also been recognized during the phase transition. On the other hand, recent reports have revealed that ultrathin VO_2 films deposited on lattice matched TiO_2 substrates show no monoclinic phase at room temperature, suggesting that the VO_2 films are tetragonal rutile in both the insulating and metallic states, i.e., the films undergo an electronic phase transition without the structural phase transition.[20–22]

The ability to tune T_{MIT} is important in many device applications.[23,24] Doping with high-valence metal ions into the VO_2 lattice is a commonly used method to achieve tuning of the T_{MIT} in VO_2 films.[25,26] Introducing epitaxial strain between

VO_2 and the substrate has also been realized as an effective way to control the T_{MIT} in VO_2 films. TiO_2 rutile substrates are most commonly used for the growth of epitaxial VO_2 films due to rutile's matching crystal structures and similar lattice parameters with metallic VO_2 (P42/mnm). Muraoka *et al.* reported that ultrathin VO_2 films show a reduced T_{MIT} (299 K) when grown on TiO_2 (001) substrates, while the T_{MIT} increased up to 369 K for VO_2 films grown on TiO_2 (110) substrates.[27] In the former case, the compressive strain in the c-axis of the VO_2 films resulted in the reduced T_{MIT} while in the latter, the tensile strain in the c-axis led to the increased T_{MIT}. Fan *et al.* also reported the thickness-dependent interfacial strain dynamics of epitaxial VO_2 films grown on TiO_2 (001) substrates, demonstrating that a large epitaxial strain occurred in the initial growth stage of the VO_2 films and the epitaxial strain was relaxed as the film thickness increased, leading to an increase in the T_{MIT}.[21] In addition, various buffer layers have been introduced between VO_2 films and substrates in order to control the strain and MIT properties in VO_2 films.[28-31] Among them, RuO_2 was proposed as an excellent buffer because it has the same crystal structure and space group as both TiO_2 and metallic VO_2.[31] In this report,[31] they showed that the T_{MIT} of thin VO_2 films can be changed continuously by epitaxial strain in a buffer layer of varying thickness. Here we report a systematic study on the epitaxial strain of VO_2 films by varying RuO_2 and VO_2 film thickness using X-ray reciprocal space mapping analysis. Furthermore, the a-axis lattice parameter of VO_2 (a = 4.54 Å, c = 2.88 Å, JCPDS #71-4821) is smaller than the TiO_2 (a=4.59 Å, c = 2.96 Å, JCPDS #21-1276) but bigger than the RuO_2 (a = 4.49 Å, c = 3.11 Å, JCPDS #40-1290), indicating that the VO_2 film can be compressively strained along the in-plane direction when deposited on bulk RuO_2 whereas it would be tensile-strained on the TiO_2 (001) substrate. Thus, the T_{MIT} in VO_2 films can be tuned by adjusting the epitaxial strain of the RuO_2 buffer layer. Another advantage of using a RuO_2 buffer layer is that it can be used as a bottom oxide electrode for VO_2 based devices with out-of-plane configurations, which would considerably reduce the switching voltage and current (compared to VO_2-based planar type devices).

In this work, we demonstrate control of the MIT temperature in VO_2 thin films by adjusting the epitaxial strain in conducting RuO_2 buffer layers. Using a 10 nm thick RuO_2/TiO_2 template, we were able to sustain the intermediate strain states even with large VO_2 film thicknesses (~100 nm), resulting in relatively low T_{MIT} (~30 °C).

II. EXPERIMENTAL METHODS

VO_2/RuO_2 thin films were epitaxially grown on single crystal TiO_2 (001) substrates by pulsed laser deposition. A pulsed laser beam generated by a KrF excimer laser (LPX300, 248 nm, and pulse duration of 30ns) was introduced into a deposition chamber through a quartz window and focused on the target. The energy density of the laser beam was 2 J/cm^2 at the target surface. A RuO_2 target (American Elements) was used for the buffer layer growth and the VO_2 films were grown from a V_2O_5 target (Kurt J. Lesker). Before thin film deposition, the chamber was evacuated to a background pressure of 10^{-5} Torr. The RuO_2 buffer layers (10 - 50 nm) were deposited at 500 °C and at 10 mTorr of oxygen partial pressure, followed by VO_2 layers (20 - 100 nm) grown at 390 °C and at 10 mTorr of oxygen. The structure of deposited films was characterized by x-ray diffraction (XRD) θ-2θ scans using a Rigaku x-ray diffractometer with Cu Kα radiation. The electrical properties of the VO_2/RuO_2 heterostructures were characterized in a probe station equipped with a heating stage (Linkam) at temperatures between 0 and 100 °C using a Keithley 4200 semiconductor characterization system.

III. RESULTS

In order to investigate the effect of the RuO_2 film thickness on the epitaxial strain of VO_2/RuO_2 heterostructures, RuO_2 buffer layers (10 - 50 nm) were prepared on TiO_2 (001) substrates while holding the VO_2 film thickness constant at 50 nm. Figure 1a shows the θ-2θ XRD patterns of the $VO_2/RuO_2/TiO_2$ thin films with various RuO_2 film thicknesses (10, 30 and 50 nm). The strong peak at 62.8° is assigned to the TiO_2 (002) substrate whereas the peak at ~60° is indexed

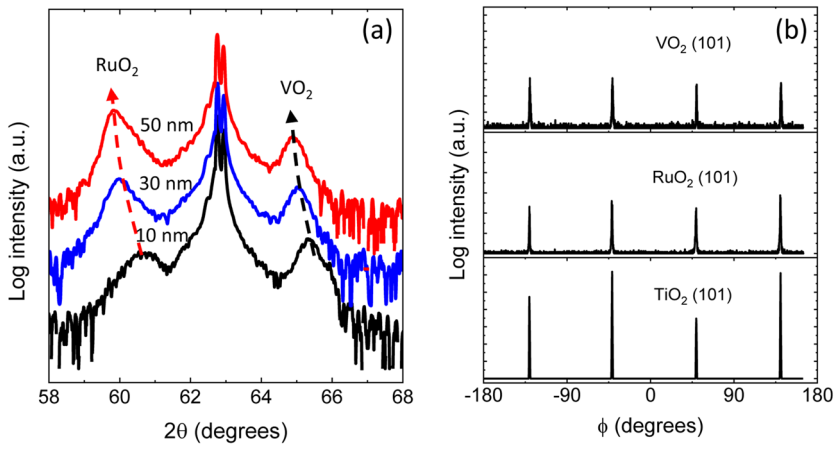

FIG. 1. (a) XRD θ-2θ patterns of VO_2(50nm)/RuO_2 thin films grown on TiO_2 (001) with three different RuO_2 thicknesses (10, 30, 50 nm). The red and black broken lines represent the trend line of RuO_2 (002) and VO_2 (002) peak positions, respectively. (b) XRD ϕ-scans of VO_2 (101), RuO_2 (101) and TiO_2 (101) peaks for VO_2 (50 nm)/RuO_2 (10 nm)/ TiO_2 heterostructure.

to rutile RuO_2 (002), and the peak at ~65° is indexed to the tetragonal VO_2 (002) plane. No other peaks were observed, indicating that pure VO_2 was formed during film growth. With increasing RuO_2 buffer layer thickness, the RuO_2 (002) peak moves to lower 2θ angles (approaching the bulk RuO_2 (002) angle) and the VO_2 (002) peak moves to lower 2θ angles (approaching the bulk VO_2 (002) angle). This result suggests that the c-axis lattice parameter of both the RuO_2 buffer layers and the VO_2 thin films increases as the RuO_2 thickness increases, meaning that the epitaxial strain can be adjusted using different thicknesses of the RuO_2 buffer layer.

XRD ϕ-scans were performed to establish the epitaxial relationship in the $VO_2/RuO_2/TiO_2$ layers. Figure 1b shows XRD ϕ-scans on VO_2 (101), RuO_2 (101) and TiO_2 (101) for the 50 nm thick VO_2 film on RuO_2 (10 nm) buffered TiO_2 substrate. The ϕ-scan of the TiO_2 exhibits four peaks separated by a 90°, suggesting fourfold symmetry about the out-of-plane axis. The ϕ-scans of the RuO_2 buffer layer and VO_2 film also show fourfold symmetry with the same azimuth angles of the TiO_2 substrate, thus showing the epitaxy of the VO_2 film on the RuO_2/TiO_2 template with a relationship of $[100]VO_2||[100]RuO_2||[100]TiO_2$ along the in-plane direction and $[001]VO_2||[001]RuO_2||[001]TiO_2$ along the out of plane direction. Four-fold symmetry of all peaks suggests that all of these materials show their characteristic tetragonal symmetry at room temperature.

In order to understand the epitaxial strain of $VO_2/RuO_2/TiO_2$ heterostructures we performed x-ray reciprocal space mapping (RSM) measurements. Figures 2a–d show the RSMs around the TiO_2 (112) peak for 50 nm thick VO_2 films on RuO_2 buffer layers with various RuO_2 thicknesses (10, 20, 30 and 50 nm). The Q_X and Q_Z values of bulk VO_2 are represented with a square symbol and the Q_X and Q_Z values of bulk RuO_2 are marked with a circular symbol. The VO_2 film on a 10 nm RuO_2 buffer layer shows that the Q_Z value of the VO_2 peak is slightly larger than the bulk Q_Z value of VO_2, suggesting that the film shows compressive strain in the c-axis. Furthermore, the Q_X value for the VO_2 peak is observed to be slightly smaller than the bulk Q_X value of VO_2, indicating that the film shows in-plane tensile strain. As the thickness of the RuO_2 buffer layer increases, the Q_X and Q_Z values of deposited VO_2 films are approaching the bulk VO_2. This shift of the diffraction positions suggests that the VO_2 film on thicker RuO_2 is more relieved that the film on thinner RuO_2. More strain is induced in the VO_2 films grown on thinner RuO_2 buffers (10-20nm) due to a decrease in the RuO_2 c-axis (compared to 50 nm RuO_2), which leads to a concomitant increase in its a-axis.

In order to investigate thickness effects on the MIT properties of VO_2, we have prepared VO_2 films with various thicknesses (20 – 100 nm) on 10 nm RuO_2 buffered TiO_2 substrates. Figures 2e–h show the RSMs data for various thicknesses of VO_2 films grown on 10 nm thick RuO_2 buffer layers. For the 20 nm thick VO_2 film, the Q_X values of the VO_2 film, RuO_2 buffer and TiO_2 substrate are almost the same, suggesting that large parts of the VO_2 film and RuO_2 buffer layer are coherently strained to the TiO_2 substrate. As the VO_2 film thickness increases, the Q_X and Q_Z values of VO_2 peaks approach those of bulk VO_2 (square symbol), indicating that the thicker VO_2 film (100 nm) is more relaxed than its thinner (20 nm) counterpart but still exhibiting a partially strained state. The streaks present in all maps are due to the saturation of the position sensitive detector. Furthermore, the RSM data for 50 nm VO_2 films grown on TiO_2 substrates with and without a RuO_2 buffer layer is also shown in Fig. S1 in the supplementary material. Notably, the $VO_2/RuO_2/TiO_2$ sample is more strained than the VO_2/TiO_2 sample.

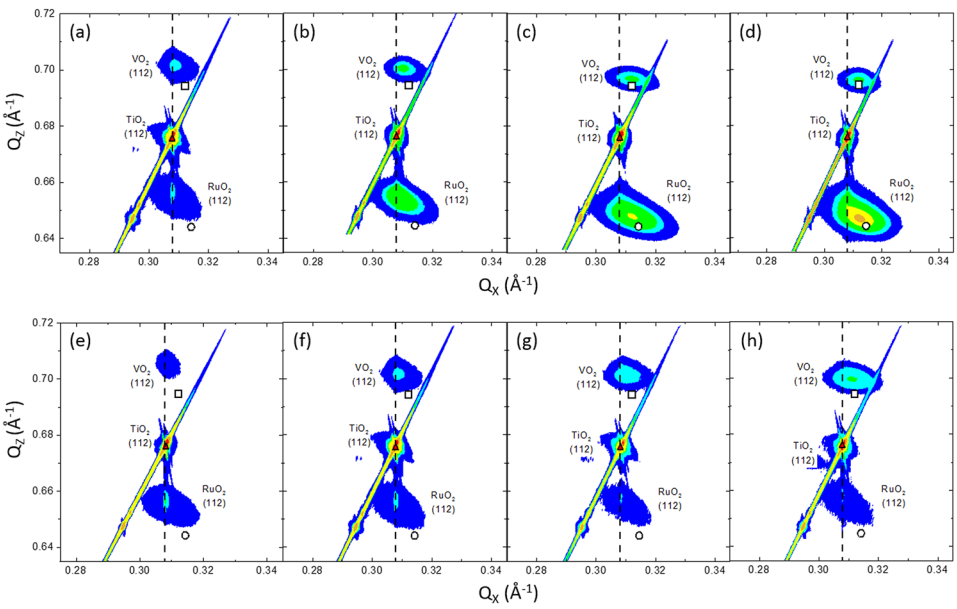

FIG. 2. (a-d) XRD RSMs of VO_2 films (50 nm) deposited on various thicknesses of RuO_2 buffer layers; (a) 10 nm, (b) 20 nm, (c) 30 nm and (d) 50 nm. (e-f) RSMs of various thicknesses of VO_2 films; (e) 20 nm, (f) 50 nm, (g) 75 nm and (h) 100 nm, deposited on 10 nm-RuO_2 buffers. All RMSs are collected around the (112) diffraction spot of TiO_2 at room temperature. The square symbols mark the Q_X and Q_Z values for bulk VO_2 (112), the triangle symbols mark the bulk TiO_2 (112), and the circular symbols mark the bulk RuO_2 (112) spot.

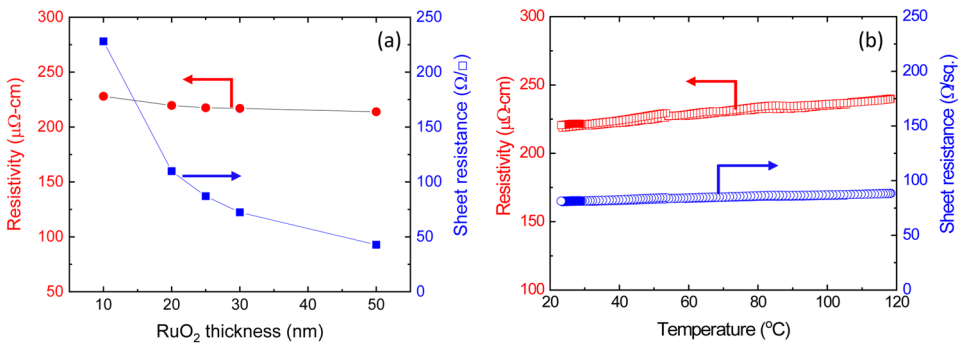

FIG. 3. (a) Room temperature resistivity and sheet resistance of RuO_2 thin films grown on TiO_2 (001) substrates as a function of the film thickness (10 - 50 nm). (b) Resistivity and sheet resistance of the RuO_2 thin film (25 nm) grown on TiO_2 (001) substrate as a function of temperature (heating and cooling).

Thickness-dependent electrical properties of the RuO_2 buffer layers were measured in order to examine the feasibility of the RuO_2 thin films as a bottom electrode. Figure 3a shows the room temperature resistivity and sheet resistance data of the RuO_2 thin films grown on TiO_2 (001) substrates as a function of the film thickness (10 - 50 nm) while the film growth temperature and oxygen pressure were fixed at 500 °C and 10 mTorr, respectively. The room temperature sheet resistance decreases from 225 to 43 Ω/□ with increasing RuO_2 film thickness from 10 to 50 nm while the film resistivity remains almost constant (~220 μΩ-cm), which is similar to that of commercial indium tin oxide (ITO) electrodes [50 nm-thick ITO films with ~50 Ω/□; ~250 μΩ-cm]. Thus, the RuO_2 buffer layers with a thickness range from 10 to 50 nm can be used as a bottom electrode for VO_2-based devices with out-of-plane configurations. Figure 3b shows the resistivity and sheet resistance of a typical RuO_2 film (25 nm) as a function of temperature (20 - 120 °C). The resistivity rises slightly from 220 to 240 μΩ-cm while increasing temperature from 20 to 120 °C. Upon cooling, the film resistivity follows the same line (during heating) with a positive slope, which is typical behavior of metals. The room temperature resistivity remains the same (220 μΩ-cm) after the cooling process. The electrical properties as a function of oxygen deposition pressure of the RuO_2 thin films are also shown in Fig. S2 in the supplementary material.

Temperature-dependent electrical transport properties were measured for VO_2 (50 nm)/RuO_2 heterostructures with varying RuO_2 buffer layer thicknesses (10 – 50 nm). The effective sheet resistance (R_{eff}) of the VO_2/RuO_2 heterostructures is shown in Fig. 4a. It shows that the T_{MIT} of all VO_2/RuO_2 films is lower than that of typical bulk VO_2 (~67 °C). The T_{MIT} surely decreases from 59 to 24 °C as the RuO_2 buffer layer thickness decreases from 50 nm to 10 nm. This reduction in T_{MIT} can be explained by a difference in epitaxial strain between the VO_2 and RuO_2 films. In general, when VO_2 films have the highest in-plane tensile epitaxial strain, the lowest T_{MIT} in the VO_2 would be expected.[21,32] Therefore, the 10 nm RuO_2 seems to be an ideal buffer layer to produce the largest epitaxial strain in VO_2 films, showing the lowest T_{MIT} (24 °C). The VO_2 films grown on thicker RuO_2 buffer layers (>10 nm) all showed higher T_{MIT}, indicating that these films are less strained than the VO_2 film on 10 nm RuO_2 buffer. It is noted that the magnitude of resistance change diminishes with increasing RuO_2 thickness. This

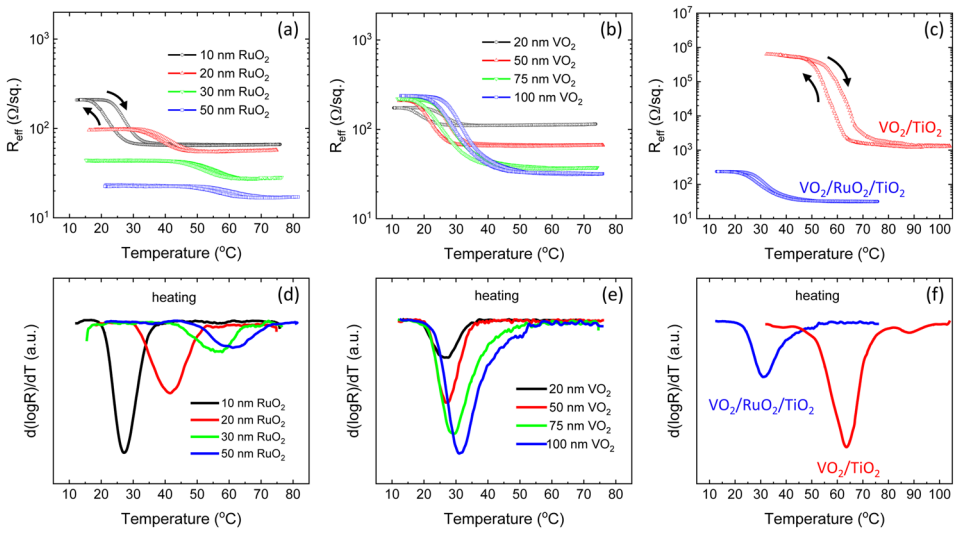

FIG. 4. (a) Effective sheet resistance vs temperature for 50 nm thick VO_2 films grown on RuO_2/TiO_2 as a function of RuO_2 buffer layer thickness (10 – 50 nm). (b) Effective sheet resistance vs temperature for various thicknesses of VO_2 films (20, 50, 75 and 100 nm) grown on RuO_2 (10 nm)/TiO_2 templates. (c) Effective sheet resistance vs temperature for 100 nm VO_2 films grown on TiO_2 substrates with/without RuO_2 buffer layer. Arrows show measurement direction. (d) - (f) Corresponding derivative curves during heating process for plots in (a), (b) and (c), respectively.

TABLE I. Transition temperatures of $VO_2/RuO_2/TiO_2$ heterostructures during heating and cooling processes. T_{heat} and T_{cool} are the transition temperatures determined from the derivative curves during heating and cooling, respectively. T_{MIT} is determined by the average between T_{heat} and T_{cool}.

Transition temperature	50 nm-VO_2 grown on TiO_2 with various thicknesses of RuO_2 buffer				Various thicknesses of VO_2 films grown on TiO_2 with 10 nm RuO_2 buffer				100 nm-VO_2 on TiO_2 with/without 10 nm RuO_2 buffer	
	10 nm	20 nm	30 nm	50 nm	20 nm	50 nm	75 nm	100 nm	With RuO_2	Without RuO_2
T_{heat} (°C)	28.3	41.6	56.2	60.7	26.7	27.3	29.1	31.2	31.2	63.6
T_{cool} (°C)	22.9	38.4	52.4	57.1	19.6	21.3	26.6	28.4	28.4	56.8
T_{MIT} (°C)	25.6	40.0	54.3	58.9	23.2	24.3	27.8	29.8	29.8	60.2

is primarily due to the low resistivity (~220 μΩ-cm) of the RuO_2 layer and the associated current shunting through the RuO_2 layer as the RuO_2 sheet resistance decreases from 225 to 43 Ω/□ with increasing RuO_2 thickness from 10 to 50 nm (shown in Fig. 3a).

The electrical transport properties were also affected by the VO_2 film thickness. Figure 4b shows temperature-dependent sheet resistance plots of VO_2 films with varying thickness (20, 50, 75 and 100 nm) while the thickness of the RuO_2 buffer layers was fixed at 10 nm. As the film thickness increases from 20 nm to 100 nm, the resistance change amplitude increases threefold, while the T_{MIT} of VO_2 films slightly increases from 23 °C to 30 °C. For comparison, the sheet resistance curves of 100 nm VO_2 films on TiO_2 substrates with and without the RuO_2 buffer layer are plotted in the same figure (Fig. 4c). Without the RuO_2 buffer layer, the T_{MIT} of the VO_2 film increases from 30 °C to 60 °C. It is clear that the 10 nm RuO_2 buffer layer is responsible for lowering the T_{MIT} by preventing relaxation of the strain on the 100 nm thick VO_2 film. Furthermore, this low T_{MIT} (30 °C) for 100 nm thick VO_2 films is ideal for operating switching devices because the transition occurs near room temperature. The T_{MIT} of VO_2 films are deduced from the derivative curves in Fig. 4d–f and are summarized in Table I.

IV. DISCUSSION

The T_{MIT} in VO_2 has been observed to be dependent on epitaxial strain in thin films.[27,33] In general, compressive strain along the c-axis of VO_2 (i.e., in-plane tensile strain) leads to a reduced T_{MIT} in epitaxial VO_2 films. Furthermore, since the a-axis lattice parameter of RuO_2 (a = 4.49 Å) is smaller than TiO_2 (a = 4.59 Å), the initial epitaxial RuO_2 film layers are subject to tensile-strains at the RuO_2/TiO_2 interface. As the thickness of RuO_2 increases, its lattice parameter monotonically decreases due to relaxation by misfit dislocations. Thus, the T_{MIT} in VO_2 films can be modified efficiently by the epitaxial strain in RuO_2 buffer layers. Figure 5a shows the axial ratio (c/a) for 50 nm-thick VO_2 films with varying RuO_2 thickness. The a- and c-axis lattice parameters of VO_2 films were calculated from RSM data. Clearly, the tendency of the c/a ratio is similar to that of the T_{MIT} in strained VO_2 films. The c/a ratio in VO_2 films decreases as the RuO_2 thickness decreases which, in turn, results in a lower T_{MIT}. The lowest T_{MIT} (24 °C) is observed in the VO_2 film having the smallest c/a ratio (for a 10 nm RuO_2 buffer layer), indicating that the VO_2 film is under tensile strain along the in-plane axis and under compressive strain along the out-of-plane axis. However, as the RuO_2 buffer layer thickness increases, its epitaxial strain becomes more relaxed and the induced strain in the VO_2 film is relieved, thus increasing the VO_2 c/a ratio, leading to an increased T_{MIT} (59 °C), closer to the bulk VO_2 value (67 °C).

Figure 5b shows the axial ratio (c/a) for VO_2 films as a function of film thickness while the RuO_2 thickness is fixed at 10 nm. As the VO_2 thickness increases from 20 to 100 nm, the c/a ratio in the VO_2 films slightly increases from 0.621 to 0.628, which is still much smaller than that of a fully relaxed VO_2 film (0.634). This low c/a ratio results in a reduced T_{MIT} (23 - 30 °C) for 20-100 nm thick VO_2 films, indicating that a significant portion of strain is still present even in 100 nm thick VO_2 films. In general, the VO_2 film is coherently strained below its critical thickness, and above the critical thickness the strained film is relaxed by the formation of misfit dislocations until it becomes fully relaxed.[34] VO_2 films grown

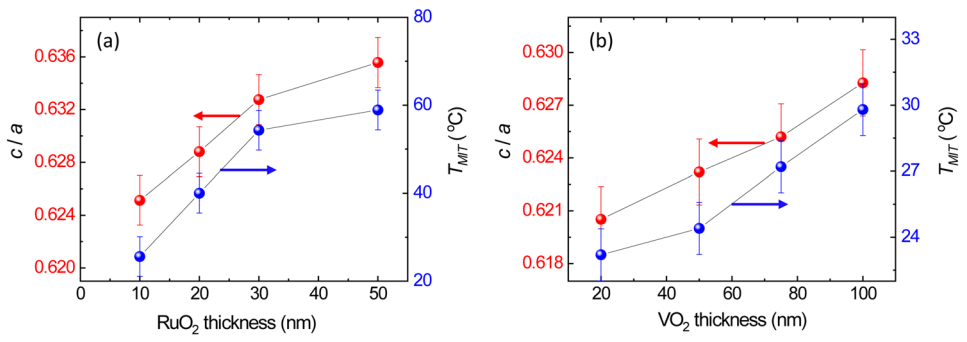

FIG. 5. (a) The axial ratio (c/a) and MIT temperature (T_{MIT}) for 50 nm VO_2 films grown on RuO_2/TiO_2 templates with various thicknesses of RuO_2 buffers (10, 20, 30 and 50 nm). (b) The axial ratio (c/a) and T_{MIT} for various thicknesses of VO_2 films (20, 50, 75 and 100 nm) grown on 10 nm RuO_2/TiO_2 templates.

on single crystal TiO_2 (001) substrates are well explained by this strain relaxation mechanism: where below 15 nm the VO_2 film is fully strained but when its thickness reaches 100 nm it is completely relaxed due to the formation of misfit dislocations.[21] However, it is difficult to explain our results on VO_2 films grown on RuO_2/TiO_2 templates using this classical strain mechanism. Instead, the strain relaxation behavior in our films can be explained by grain boundaries. The grain size of the RuO_2 buffer layer was determined by atomic force microscopy to be ~ 30 – 40 nm as shown in Fig. S3 in the supplementary material. The boundary between RuO_2 grains is a favorable region for dislocation nucleation. Thus, high density boundaries in RuO_2 buffer layers can provide an alternative pathway to relieve the strain at the VO_2/RuO_2 interface. This explains why our VO_2 films can sustain intermediate strain states for thicker films up to 100 nm. Similar results (strain relaxation through grain boundaries) have been reported for other epitaxial oxide systems.[29,35–38] It is worth pointing out that 100 nm-thick VO_2 films grown on conducting RuO_2 electrodes can still provide a lower T_{MIT} (~30 °C) presumably due to residual strain induced by the RuO_2 buffer layer. Hence, VO_2 based devices with an out-of-plane configuration can be realized at near room temperature using 100 nm thick VO_2 films and 10 nm thick RuO_2 electrodes.

V. CONCLUSIONS

Epitaxial VO_2 thin films were deposited on conductive RuO_2/TiO_2 templates by pulsed laser deposition. The MIT temperature of $VO_2/RuO_2/TiO_2$ heterostructures can be tuned from 59 °C to 24 °C by adjusting the strain state of the films by decreasing the RuO_2 thickness from 50 nm to 10 nm. The boundaries between RuO_2 structures are favorable regions responsible for the nucleation of dislocations, which can partially relieve the strain in the film, thereby sustaining intermediate strain states even with large thicknesses (~100 nm). This allows lowering of the MIT temperature to near room temperature. These results suggest that the strain generated by the RuO_2 buffer layer can provide an effective way for tuning the T_{MIT} of VO_2 films and provide a route to realizing out-of-plane electrical switching devices.

SUPPLEMENTARY MATERIAL

See supplementary material for the RSMs data, electrical properties and AFM images.

ACKNOWLEDGMENTS

This work was funded by the Office of Naval Research (ONR) through the Naval Research Laboratory Basic Research Program.

REFERENCES

[1] F. J. Morin, Phys. Rev. Lett. **3**, 34 (1959).
[2] D. H. Kim and H. S. Kwok, Appl. Phys. Lett. **65**, 3188 (1994).
[3] J. Sakai and M. Kurisu, Phys. Rev. B. **78**, 033106 (2008).
[4] A. Cavalleri, C. Tóth, C. Siders, J. Squier, F. Ráksi, P. Forget, and J. C. Kieffer, Phys. Rev. Lett. **87**, 237401 (2001).
[5] R. J. Suess, N. S. Bingham, K. M. Charipar, H. Kim, S. A. Mathews, A. Piqué, and N. A. Charipar, Adv. Mater. Interfaces 1700810 (2017).
[6] M. F. Jager, C. Ott, P. M. Kraus, C. J. Kaplan, W. Pouse, R. E. Marvel, R. F. Haglund, D. M. Neumark, and S. R. Leone, PNAS **114**(36), 9558 (2017).
[7] H. Kim, N. Charipar, M. Osofsky, S. B. Qadri, and A. Piqué, Appl. Phys. Lett. **104**, 081913 (2014).
[8] N. A. Charipar, H. Kim, S. A. Mathews, and A. Piqué, AIP Advances **6**, 015113 (2016).
[9] A. Pashkin, C. Küber, H. Ehrke, R. Lopez, A. Halabica, R. F. Haglund, R. Huber, and A. Leitenstorfer, Phys. Rev. B **83**, 195120 (2011).
[10] H. Kim, N. Charipar, E. Breckenfeld, A. Rosenberg, and A. Piqué, Thin Solid Films **596**, 45 (2015).
[11] N. Shukla, A. V. Thathachary, A. Agrawal, H. Paik, A. Aziz, D. G. Schlom, S. K. Gupta, R. Engel-Herbert, and S. Datta, Nat. Comms. **6**, 7812 (2015).
[12] Y. Zhou and S. Ramanathan, J. Appl. Phys. **111**, 084508 (2012).
[13] H. Takeya, J. Frame, T. Tanaka, Y. Urade, X. Fang, and W. Kubo, Sci. Rep. **8**, 12764 (2018).
[14] D. W. Ferrara, J. Nag, E. R. MacQuarrie, A. B. Kaye, and R. F. Haglund, Jr., Nano Lett **13**, 4169 (2013).
[15] K. Liu, C. Cheng, J. Suh, R. T-Kong *et al.*, Adv. Mater. **26**, 1746 (2014).
[16] A. Hendaoui, N. Émond, S. Dorval, M. Chaker, and E. Haddad, Solar Energy Materials & Solar Cells **117**, 494 (2013).
[17] H. Kim, T. V. Slusar, D. Wulferding, I. Yang, J.-C. Cho, M. Lee, H. C. Choi, Y. H. Jeong, H.-T. Kim, and J. Kim, Appl. Phys. Lett. **109**, 233104 (2016).
[18] K. Okimura, T. Watanabe, and J. Sakai, J. App. Phys. **111**, 073514 (2012).
[19] S. Lee, I. N. Ivanov, J. K. Keum, and H. N. Lee, Scientific Reports **6**, 19621 (2016).
[20] M. Yang, Y. Yang, B. Hong, L. Wang, K. Hu, Y. Dong, H. Xu, H. Huang, J. Zhao, H. Chen, L. Song, H. Ju, J. Zhu, J. Bao, X. Li, Y. Gu, T. Yang, X. Gao, Z. Luo, and C. Gao, Sci. Rep. **15**, 23119 (2016).
[21] L. L. Fan, S. Chen, Z. L. Luo, Q. H. Liu, Y. F. Wu, L. Song, D. X. Ji, P. Wang, W. S. Chu, C. Gao, C. W. Zou, and Z. Y. Wu, Nano Lett **14**, 4036–4043 (2014).
[22] S. Kittiwatanakul, S. A. Wolf, and J. Lu, Appl. Phys. Lett. **105**, 073112 (2014).
[23] J. B. Cao, W. Fan, Q. Zhou, E. Sheu, A. W. Liu, C. Barrett, and J. Wu, J. Appl. Phys. **108**, 083538 (2010).
[24] B. J. Kim, Y. W. Lee, B. G. Chae, S. J. Yun, S. Y. Oh, H. T. Kim, and Y. S. Lim, Appl. Phys. Lett. **90**, 023515 (2007).
[25] X. Tan, T. Yao, R. Long, Z. Sun, Y. Feng, H. Cheng, X. Yuan, W. Zhang, Q. Liu, C. Wu, Y. Xie, and S. Wei, Sci. Rep. **2**, 466 (2012).
[26] K. L. Holman, T. M. McQueen, A. J. Williams, T. Klimczuk, P. W. Stephens, H. W. Zandbergen, Q. Xu, F. Ronnig, and R. J. Cava, Phys. Rev. B **79**, 245114 (2009).
[27] Y. Muraoka and Z. Hiroi, Appl. Phys. Lett. **80**, 583 (2002).
[28] H. Kim, N. S. Bingham, N. A. Charipar, and A. Piqué, AIP Advances **7**, 105116 (2017).
[29] E. Breckenfeld, H. Kim, K. Burgess, N. Charipar, S.-F. Cheng, R. Stroud, and A. Piqué, ACS Appl. Mater. Interfaces **9**, 1577 (2017).
[30] J. Jian, X. Wang, L. Li, M. Fan, W. Zhang, J. Huang, Z. Qi, and H. Wang, ACS Appl. Mater. Interfaces **9**, 5319 (2017).
[31] N. B. Aetukuri, A. X. Gray, M. Drouard, M. Cossale, L. Gao, A. H. Reid, R. Kukreja, H. Ohldag, C. A. Jenkins, E. Arenholz, K. P. Roche, H. A. Dürr, M. G. Samnt, and S. P. Parkin, Nature Physics **9**, 661 (2013).
[32] H. Qiu, M. Yang, Y. Dong, H. Xu, B. Hong, Y. Gu, Y. Yang, C. Zou, Z. Luo, and C. Gao, New J. Phys. **17**, 113016 (2015).
[33] J. Cao, E. Ertekin, V. Srinivasan, W. Fan, S. Huang, H. Zheng, J. W. L. Yim, D. R. Khanal, D. F. Ogletree, J. C. Grossman, and J. Wu, Nature Nanotechnology **4**, 732 (2009).
[34] J. W. Matthews and A. E. Blakeslee, J. Cryst. Growth **72**, 118 (1974).
[35] Y. Ding, J. Chen, J. He, M. Liu, C. Ma, and C. Chen, J. Cryst. Growth **383**, 19–24 (2013).
[36] Y. B. Chen, M. B. Matx, and X. Q. Pan, Appl. Phys. Lett. **91**, 031902 (2007).
[37] J. Q. He, E. Vasco, R. Dittmann, and R. H. Wang, Phys. Rev. B: Condens. Matter Mater. Phys. **73**, 125413 (2006).
[38] J. Narayan and V. M. Bhosle, J. Appl. Phys. **100**, 103524 (2006).